# Design and Optimization of Two-Loop Pilot for Tactical Missile

Xitong Sun, Xingbai Luo, Min Gao, Xiaodong Zhou, Wencui Zhou

*Abstract*—**The specific scheme of two-loop attitude control system was formulated based on the design principle of attitude control system with the damping circuit as the inner loop and the overload control loop as the outer one. As required by the formulated scheme, the damping loop is designed firstly, of which the stability and the dynamic response quality are improved by adjusting the damping coefficient and the addition of the correction network. After that, the design and optimization of the overload control loop are implemented. With the same design method, gain coefficient and correction network are introduced to reduce overshoot of overload response curve, shorten response time and improve efficiency. Besides, the validity of the overload control loop is tested with square wave as input to reflect the real overload command signal.**

*Index Terms*—**Autopilot; Damping Loop; Overload Control Loop; Attitude Control**

## I. Introduction

The core task of autopilot is to ensure that the missile tracks the input command generated by the guidance system accurately and robustly. Meanwhile, it makes the missile produce control torque and force based on the control command for the change of the attack angle. The direction of velocity vector is then altered to achieve stable fly of the missile before hitting the target. The multi-functionality of the new generation of advanced tactical missiles and the diversification of strike missions have placed new requirements on autopilots, such as providing large angle of attack, high maneuverability, and ensuring the robustness of a wide range of flight missions. At present, there are two kinds of autopilots that are widely used, i.e., the overload pilot and the angle control pilot. Distinguished by different control parameters, the angle control pilot follows the tracking guidance law for velocity or projectile, while the overload one utilizes the proportional navigation guidance law in most cases. For example, the American "Sparrow" air-to-air missile is equipped with the classic overload pilot.

Autopilot is of great significance to the stability control of aircraft, which is available for the compensation to the aerodynamic parameters and the changes of aircraft parameters to stabilize the aerodynamic gain. Besides, it enhances the damping characteristics of the aircraft around the mass center angle, and improves the quality of the transition process. On the other hand, autopilot offers higher response frequency to the aircraft to ensure the guidance accuracy, and mitigates the influence of cross coupling between channels, thus increasing the anti-interference ability of the system.

The classical control theory is mainly used in the design of traditional missile autopilot, in which the control parameters in line with the performance index are obtained by empirical equation and fitting method. These methods are characterized by high requirements on experience, and pretty long optimization cycle. In recent years, though many new missile autopilots based on modern control theory have been proposed, such as robust control autopilot, neural network autopilot, dynamic inversion control autopilot, singular perturbation margin autopilot and reinforcement learning autopilot[1-10] with novel and improved performance, the design of these methods has not been widely used. An optimization method is proposed in this paper for the traditional missile two-loop pilot based on time domain and frequency domain analysis, which is applied to the actual design of autopilot, and available to improve the design efficiency of control parameters.

As a common type of overload pilot, the two-loop pilot is able to change the angular rate, thereby stabilizing the attitude of the missile, and improving the quality of the transition process of the guidance system. The response efficiency of overload command is improved through the control of overload. Besides, in this paper, the system response characteristics and frequency domain characteristics are analyzed through the scheme design, theoretical derivation and mathematical simulation. In the meantime, the comparison in terms of overshoot, rise time, amplitude margin and stability margin are done for the design and optimization of the two-loop pilot of guided mortar, thus providing a reference for the selection and design of the aircraft's overload pilot.

## II. Peturbed Motion Equations

In the process of linearizing the perturbed motion equations, the following hypothesis are proposed:

(1) In the undisturbed motion, the derivatives of lateral motion parameters, i.e., $\psi_v, \psi, \beta, \gamma_V, \gamma$ and the longitudinal

Manuscript received July 08, 2020; revised December 29, 2020.

Xitong Sun is a doctor student in Ammunition Engineering Department, Army Engineering University, No. 97 Heping West Road, Shijiazhuang, Hebei, 050003, China. (e-mail: 417006576@qq.com)

Xingbai Luo is a professor in Ammunition Engineering Department, Army Engineering University, No. 97 Heping West Road, Shijiazhuang, Hebei, 050003, China. (e-mail: gli210035@gmail.com)

Min Gao is a professor in Missile Engineering Department, Army Engineering University, No.97 Heping West Road, Shijiazhuang, Hebei, 050003, China. (e-mail: gaomin1100@163.com)

Xiaodong Zhou is a professor in Ammunition Engineering Department, Army Engineering University, No. 97 Heping West Road, Shijiazhuang, Hebei, 050003, China. (corresponding author, phone: 18515661302, e-mail: zhouxiaodong202010@163.com)

Wencui Zhou is an engineer in Beijing Aerospace Flight Control Center, No. 26 Beiqing Road, Haidian District, Beijing 100094, China. (e-mail: 984028049@qq.com)

motion parameters to time are rather small. Besides the product between them and that of these parameters as well as other small quantities are omitted.

(2) The impact of the structural parameters of the projectile, atmospheric pressure, atmospheric density deviation and coordinate deviation on the disturbance motion need not to be taken into consideration.

(3) The inertial principal axis of the projectile body coincides with its geometric center axis, and the moment of inertia to any transverse axis of the mass center is equal.

(4) Aerodynamics characteristics are axisymmetric, and the aerodynamic characteristics of the projectile remain unchanged when the longitudinal axis of the projectile rotates at any angle.

(5) Rotating angular velocity of the projectile is the same in either disturbed or undisturbed movement.

(6) The influence of washing delay on motion characteristics is ignored.

Based on the above assumptions, the linearized perturbation motion equations are obtained as follows:

$$\begin{cases} \dfrac{\mathrm{d}\Delta V}{\mathrm{d}t} = \dfrac{-X^V}{m}\Delta V + \dfrac{-X^\alpha}{m}\Delta\alpha - g\cos\theta\Delta\theta + \dfrac{F_{gx}}{m} \\ \dfrac{\mathrm{d}\Delta\theta}{\mathrm{d}t} = \dfrac{Y^V}{mV}\Delta V + \dfrac{Y^\alpha}{mV}\Delta\alpha + \dfrac{g}{V}\sin\theta\Delta\theta + \dfrac{Y^{\delta_z}}{mV}\Delta\delta_z + \dfrac{F_{gy}}{mV} \\ \dfrac{\mathrm{d}\Delta\omega_z}{\mathrm{d}t} = \dfrac{M_z^V}{J_z}\Delta V + \dfrac{M_z^\alpha}{J_z}\Delta\alpha + \dfrac{M_z^{\dot\alpha}}{J_z}\Delta\dot\alpha + \dfrac{M_z^{\omega_z}}{J_z}\Delta\omega_z \\ + \dfrac{M_z^{\delta_z}}{J_z}\Delta\delta_z + \dfrac{M_{gz}}{J_z} \\ \dfrac{d\Delta\psi}{dt} = \dfrac{\Delta\omega_y}{\cos\varphi} \\ \dfrac{\mathrm{d}\Delta x}{\mathrm{d}t} = \Delta V\cos\theta + V\sin\theta\Delta\theta \\ \dfrac{\mathrm{d}\Delta y}{\mathrm{d}t} = \Delta V\sin\theta + V\cos\theta\Delta\theta \\ \Delta\theta = \Delta\varphi - \Delta\alpha \end{cases} \tag{1}$$

Where, $\Delta\delta_z'$ and $\Delta\delta_y'$ refer to the equivalent pitch rudder angle and equivalent yaw rudder angle respectively. $X^V$ refers to the simplified representation of partial derivatives used to represent $\partial X/\partial V$. The same is true for other parameters of $Y^V$, $Z^\beta$, etc.

The dynamic coefficient symbol is used to represent the coefficients in the equations to facilitate writing. The equations and motion parameter biases were numbered, as shown in Table I.

TABLE.I
DYNAMIC COEFFICIENT

| Dynamic Coefficient | Expression | Dynamic Coefficient | Expression |
|---|---|---|---|
| $a_{22}$ | $a_{22}=\dfrac{m_z^{w_z}qSl^2}{J_zV}$ | $a_{33}$ | $a_{33}=\dfrac{g\sin\theta}{V}$ |
| $a_{24}$ | $a_{24}=\dfrac{m_z^{\alpha}qSl}{J_z}$ | $a_{34}$ | $a_{34}=\dfrac{C_y^{\alpha}qS}{mV}$ |
| $a_{25}$ | $a_{25}=\dfrac{m_z^{\delta_z}qSl}{J_z}$ | $a_{35}$ | $a_{35}=\dfrac{C_y^{\delta_z}qS}{mV}$ |
| $a_{26}$ | $a_{26}=\dfrac{1}{J_z}$ | $a_{36}$ | $a_{36}=\dfrac{1}{mV}$ |

## III. DESIGN PRINCIPLE OF ATTITUDE CONTROL SYSTEM

The following principles should be followed at the time of the attitude control system design:

(1) Good dynamic characteristics and stability margin

It is pointed out in Reference [11] that the transition process of mortar projectile is the shortest at the relative damping coefficient of 0.7 which is, therefore, roughly selected in the design of damping loop. The requirements of stability margin can refer to the indexes proposed in Reference [11], i.e., amplitude margin >8dB and phase margin >60 deg (60º).

(2) The correction network should be furnished with certain adaptability

A fixed correction network is used to decrease the complexity of attitude control system due to the fact that the characteristics of mortar projectile change gently during the flight. Besides, it is designed at the point of maximum natural frequency to ensure the adaptability of the correction network.

(3) The attitude control coefficient should be furnished with certain margin

Because the theoretical control coefficient is used in the design process of attitude control system, there may be some deviations between the actual control coefficient used in the missile borne control system and the control coefficient used in the design process. Generally, the attitude control system still shows a good stability margin when the attitude control coefficient changes from - 30% to 30%.

## IV. DESIGN OF ATTITUDE CONTROL SYSTEM

The attitude control system has a significant influence on the maneuverability and interference suppression ability of the mortar projectile, which presents the basis of the guidance and control of the guided mortar. Besides, its main functions are described as follows: stabilizing the angular position or angular velocity of the projectile's axis in space; improving the damping characteristics of the projectile's motion around the center of mass and improving the quality of the transition process of the guidance system; stabilizing the static transfer coefficient and dynamic characteristics of the mortar projectile; and executing the guidance command by controlling the mass center of the mortar projectile to fly along the reference trajectory.

Due to the limitation of aerodynamic configuration and the impossibility to select too large wing area, the relative damping coefficient of mortar projectile is usually small, that is, about 0.1 or even smaller. Even if the mortar projectile is stable, violent oscillation and overshoot will still be generated due to the interference, which will increase the angle of attack and the miss distance; while in the meantime, reduce the range and the tracking accuracy. In general, in the attitude control system, it is necessary to modify the damping characteristics of the missile body to increase the damping of the missile body, that is, an angular rate gyroscope is added to the missile, and the angular velocity of the missile body is taken as the feedback to construct the damping loop. In the attitude control system, the damping loop acts as the inner loop, while the outer loop refers to the overload control loop which takes the acceleration of the projectile as the feedback information.

Among them, the attitude angle information is obtained by MEMS gyroscope output signal, and the acceleration information is measured by the accelerometer. Besides, the schematic diagram of the attitude control system is shown in Fig. 1.

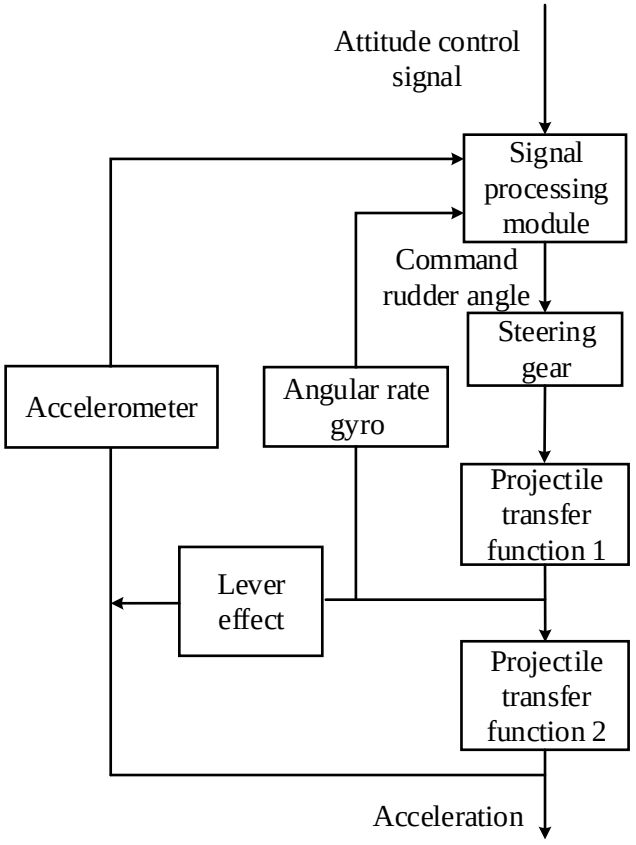


Fig.1 Schematic diagram of attitude control system

Being axisymmetric in most cases, the pitch channel and yaw channel of the guided mortar have the same dynamic characteristics. In this paper, only the pitch channel is taken as an example for the design of the attitude control system.

By means of the analysis of the whole ballistic dynamic coefficient of guided ammunition, the point with the maximum fixed frequency is selected as the eigenvalue point, and the relevant dynamic coefficients of this point are obtained as follows:

TABLE.II
NUMERICAL VALUES OF DYNAMIC COEFFICIENTS AT EIGENVALUE POINTS

| Dynamic Coefficient | Value |
|---|---|
| $a_{22}$ | -5.5406 |
| $a_{24}$ | -1445.2149 |
| $a_{25}$ | -316.1307 |
| $a_{34}$ | 0.8110 |
| $a_{35}$ | $3.6463\times10^{-5}$ |

*A. Transfer function of steering gear*

Following the working principle of the actuator system, its transfer function can be expressed by a second-order oscillation link, as expressed below:

$$G_{dj}=\frac{K_{dj}}{T_{dj}{}^2s^2+2\xi_{dj}T_{dj}s+1} \tag{2}$$

Where $K_{dj}$ refers to the steering gear amplification factor, $T_{dj}$ refers to the steering gear time constant, and $\xi_{dj}$ refers to the steering gear damping coefficient.

The steering gear of guided mortar projectile can be expressed by the following model:

$$G_{dj}=\frac{1}{\frac{1}{220^2}s^2+2\cdot0.65\cdot\frac{1}{220}s+1} \tag{3}$$

*B. Projectile Transfer Function 1*

The projectile transfer Function 1 takes pitch rudder angle as the input and pitch attitude angular velocity as the output.

$$G_{\delta_z}^{\dot{\vartheta}}=\frac{K_M(T_{M1}s+1)}{T_M^2s^2+2T_M\xi_Ms+1} \tag{4}$$

Where $K_M$ refers to the transmission coefficient of the missile body; $T_M$ refers to the time constant of the missile body; $T_{M1}$ refers to the aerodynamic time constant of the missile body, and $\xi_M$ refers to the damping coefficient of the missile body. The calculation method is expressed as follows:

$$\begin{cases}K_M=\dfrac{-a_{25}a_{34}+a_{35}a_{24}}{a_{22}a_{34}+a_{24}}\\ T_M=\dfrac{1}{\sqrt{-a_{24}-a_{22}a_{34}}}\\ \xi_M=\dfrac{-a_{22}+a_{34}}{2\sqrt{-a_{24}-a_{22}a_{34}}}\\ T_{M1}=\dfrac{a_{25}}{a_{25}a_{34}-a_{35}a_{24}}\end{cases} \tag{5}$$

*C. Projectile Transfer Function 2*

The projectile transfer Function 2 takes pitch attitude angular velocity as the input and acceleration (overload) as the output, as expressed below:

$$G_{\dot{\vartheta}}^{a_y}=\frac{V(A_2s^2+A_1s+1)}{T_{M1}s+1} \tag{6}$$

Where, $V$ refers to the velocity of guided ammunition.

In the formula, the expressions of $A_2$ and $A_1$ are as follows:

$$\begin{cases}A_2=\dfrac{a_{35}}{a_{25}a_{34}-a_{35}a_{24}}\\ A_1=\dfrac{-a_{35}a_{22}}{a_{25}a_{34}-a_{35}a_{24}}\end{cases} \tag{7}$$

*D. Transfer function of inertial assembly*

According to the working principle of MEMS gyroscope, the general form of its transfer function is expressed as follows:

$$G_{Js}=\frac{K_{Js}}{T_{Js}{}^2s^2+2\xi_{Js}T_{Js}s+1} \tag{8}$$

The transfer function of the angular rate gyro used in the attitude control system is expressed as follows:

$$G_{Js}=\frac{1}{\frac{1}{500^2}s^2+2\cdot 0.65\cdot\frac{1}{500}s+1} \tag{9}$$

*E. Accelerometer transfer function*

Based on the working principle of accelerometer, the general form of its transfer function is expressed as follows:

$$G_J=\frac{K_j}{T_J{}^2s^2+2\xi_J T_J s+1} \tag{10}$$

The transfer function of the accelerometer used in the attitude control system is expressed as follows:

$$G_J=\frac{1}{\frac{1}{500^2}s^2+2\cdot 0.65\cdot\frac{1}{500}s+1} \tag{11}$$

## V. Design of Attitude Control Loop for Pitch Channel

The function of pitch channel attitude control loop is used to enhance the damping characteristics of missile body, and make the normal acceleration of missile body follow the input command acceleration control signal. Its structure is shown in Fig. 2.

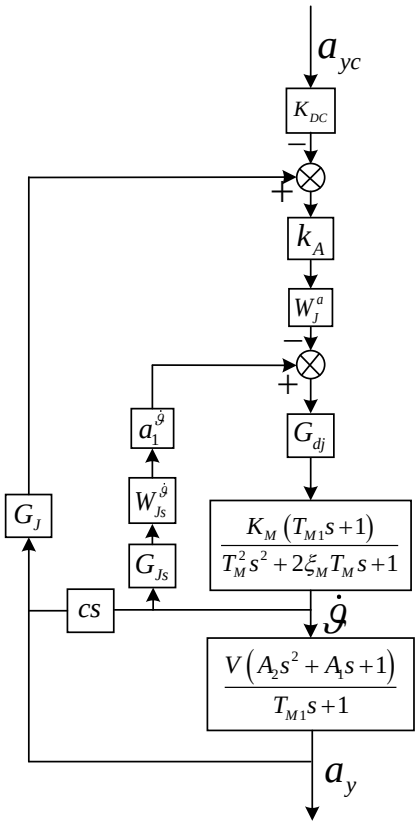


Fig.2 Structure diagram of attitude control loop for pitch channel

Where, $a_{yc}$ represents the input acceleration control signal; $G_{dj}$ represents the transfer function of the servo; $G_{Js}$ represents the transfer function of the MEMS gyroscope; $a_1^{\dot\vartheta}$ and $W_{Js}^{\dot\vartheta}$ represent the gain and correction network of the damping loop respectively; $k_A$ and $W_J^a$ represent the gain and correction network of the acceleration control loop respectively; and $\dot\vartheta$ and $a_y$ represent the pitch angular velocity and normal acceleration of the projectile respectively. Besides, $K_{DC}$ is used to adjust the overall attitude control loop gain to 1. While c refers to the distance from the accelerometer installation position to the center of mass. Accelerometer c is positive before the centroid, otherwise it is negative.

Where $a_{yc}$ represents the input acceleration control signal; $G_{dj}$ represents the transfer function of the steering gear; $G_{Js}$ represents the transfer function of MEMS gyroscope; $a_1^{\dot\vartheta}$ and $W_{Js}^{\dot\vartheta}$ represent the gain and correction network of the damping loop, respectively; $k_A$ and $W_J^a$ represent the gain and correction network of the acceleration control loop, respectively; $\dot\vartheta$ and $a_y$ represent the pitch angular velocity and normal acceleration of the missile body respectively; besides, $K_{DC}$ is used to adjust the gain of the whole attitude control loop to 1; while $c$ refers to the distance between the accelerometer installation position and the center of mass, which is positive before the center of mass and goes negative after the center of mass.

For the pilot equipped with accelerometer, in the case that the installation position of accelerometer does not coincide with the center of mass, the arm effect of accelerometer should be considered to be caused by missile attitude motion. In other words, if the accelerometer is not installed at the center of mass, the accelerometer measurement information will contain the attitude angle acceleration information due to the influence of attitude angle motion, which should be removed during data processing.

*A. Design of the damping loop*

The design of damping loop is divided into static design and dynamic design. For the former, the gain coefficient is determined based on the known transfer coefficient of each link, therefore, the equivalent damping coefficient is maintained at a good level. While the latter is used to make sure that the damping loop is characterized by considerable stability margin and good dynamic quality through the design of correction network. The structure of the damping loop is shown in Fig. 3.

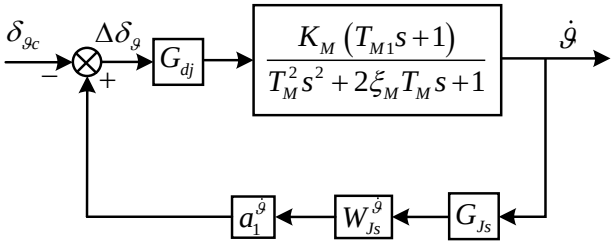


Fig.3 Structural diagram of pitch damping loop

In the initial design process, when taking into consideration that the bandwidth of the actuator and MEMS gyroscope is far greater than the natural frequency of the projectile, these two links can be regarded as non-inertial amplification links, i.e., $G_{dj}=1, G_{Js}=1$. The correction network is not considered temporarily. The closed-loop transfer function of damping loop is expressed as follows:

$$G_Z = \frac{\frac{K_M}{1+a_1^{\dot{\vartheta}}K_M}\left(T_{M1}s+1\right)}{\frac{T_M^2}{1+a_1^{\dot{\vartheta}}K_M}s^2+\frac{2\xi_M T_M + a_1^{\dot{\vartheta}}K_M T_{M1}}{1+a_1^{\dot{\vartheta}}K_M}s+1} = \frac{K_c\left(T_{M1}s+1\right)}{T_c^2 s^2+2\xi_c T_c s+1} \tag{12}$$

Where $K_c$ refers to the equivalent amplification factor; $T_c$ refers to the equivalent time constant and $\xi_c$ refers to the equivalent damping. Their calculation methods are expressed as follows (13):

$$\begin{cases} K_c = \dfrac{K_M}{1+a_1^{\dot{\vartheta}}K_M} \\ T_c = \dfrac{T_M}{\sqrt{1+a_1^{\dot{\vartheta}}K_M}} \\ \xi_c = \dfrac{2\xi_M T_M + a_1^{\dot{\vartheta}}K_M T_{M1}}{2T_M \cdot \sqrt{1+a_1^{\dot{\vartheta}}K_M}} \end{cases} \tag{13}$$

$a_1^{\dot{\vartheta}}K_M << 1$, therefore:

$$\xi_c \approx \xi_M + \frac{a_1^{\dot{\vartheta}}K_M T_{M1}}{2T_M} \tag{14}$$

$$a_1^{\dot{\vartheta}} \approx \frac{2T_M\left(\xi_c - \xi_M\right)}{K_M T_{M1}} \tag{15}$$

It is pointed out that the shortest transition process of the damping loop is obtained when the equivalent damping is $\xi_c \approx 0.707$ . Besides, $a_1^{\dot{\vartheta}} = -0.1502$ can be calculated by substituting it into Equation (15).

Through Formula (13), we can obtain: $K_c = -0.1722$ , $T_c = 0.0259$ , $\xi_c = 0.7801$.

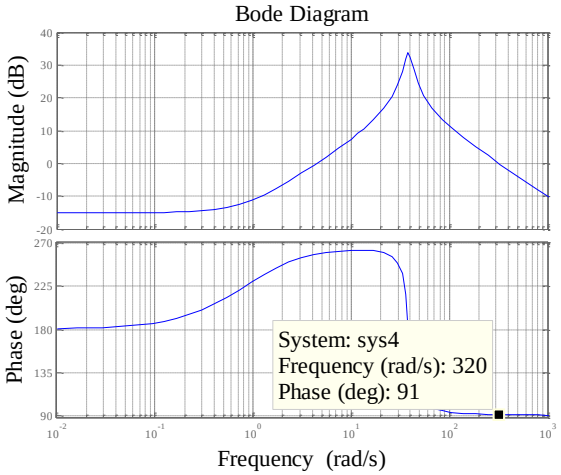


Fig.4 Frequency characteristic curve of projectile transfer function (uncorrected network, $G_{dj}=1$ , $G_{gz}=1$ )

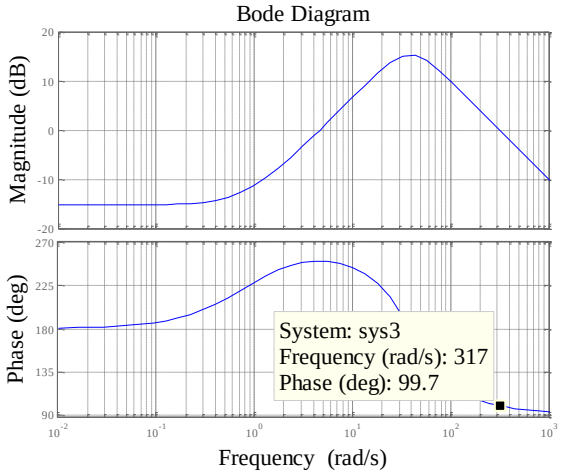


Fig.5 Frequency characteristic of pitch damping loop (adjust damping, uncorrected network, $G_{dj}=1$ , $G_{gz}=1$ )

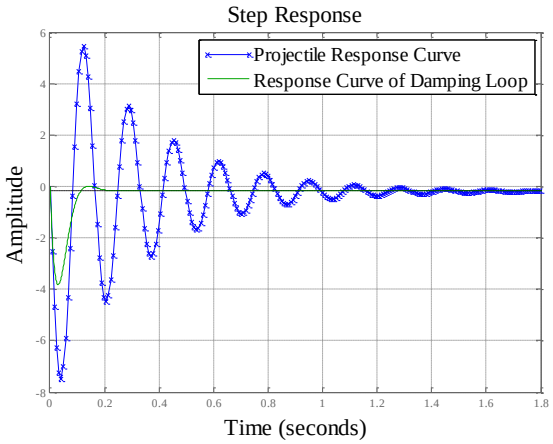


Fig.6 Unit step response curve of projectile transfer function and damping loop (uncorrected network, $G_{dj}=1$ , $G_{gz}=1$ )

As shown in Fig. 4, it can be seen from the frequency characteristic curve of missile body transfer function, that the phase angle stability margin of damping circuit is 271 deg., and the stability is good. On the other hand, it can be seen from the frequency characteristic curve of the damping loop shown in Fig. 5, that the phase angle stability margin of the damping loop is 279.7 deg., and the phase angle stability margin is improved by adjusting the loop damping.

As shown in Fig. 6, it can be seen from the unit step response curve of the projectile transfer function and the damping loop, that the projectile transfer function and the damping loop are characterized by the same steady-state response value, however, the damping loop has better dynamic characteristics. In addition, the peak value of projectile transfer function response is -7.47, and the response is with multiple oscillation cycles, while the peak value of damping loop response is -4 without any periodic oscillation.

The existence of inertia of steering gear and inertial components in practical application makes it necessary to replace the transfer functions of the actuator and inertial components into the damping loop, thus analyzing their frequency domain characteristics. Fig. 7 shows the frequency characteristic curve of damping loop when the transfer function of steering gear and inertial components is added.

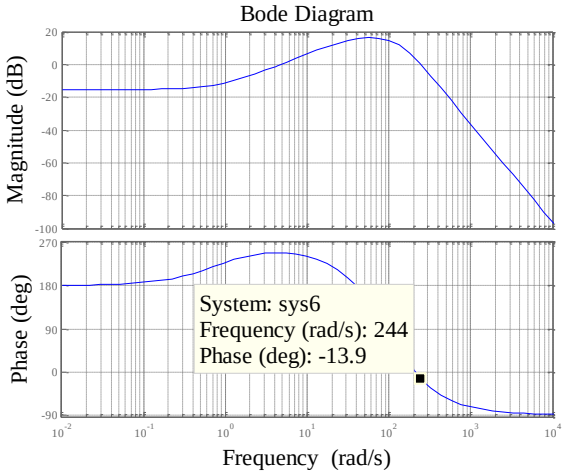


Fig.7 Frequency characteristic of pitch damping loop (adjust damping, uncorrected network)

It can be seen from Fig. 7 that the amplitude margin of the damping loop can be regarded as infinite, and the phase angle stability margin is 166.1 deg., which meets the design requirements of attitude control loop. It is found in the design process of damping loop that the addition of correction network into the feedback channel can further enhance the time domain response characteristics of damping loop, so as to improve the stability of damping loop.

*B. PID adjustment method*

Thanks to its simple algorithm, good robustness and high reliability, PID control is widely used for process control and motion control[12-14], especially in the deterministic control system which can be used to establish accurate mathematical model.

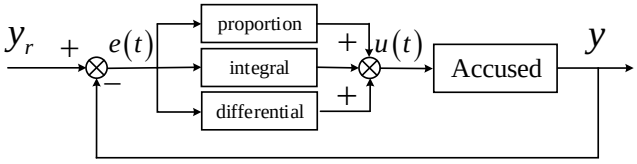


Fig.8 Principle block diagram of PID control system

The principle block diagram of PID control system is shown in Fig. 8. Besides, in the process control, the PID controller controlled by the proportion (P), integral (I) and differential (d) of deviation is the most widely used automatic controller, which is characterized by the advantages of simple principle, easy implementation, wide application range, independent control parameters and simple selection of parameters.

The output signal of the controller is expressed as follows:

$$u(t) = K_P\left(e(t) + K_I\int_0^t e(t)d\tau + K_D\frac{de(t)}{dt}\right) \tag{16}$$

The corresponding transfer function model is expressed as follows:

$$W_{Js}^{\dot{\vartheta}} = K_P\left(1 + \frac{K_I}{s} + K_D s\right) \tag{17}$$

After repeated calculation, the final correction network of damping loop is determined as follows:

$$W_{Js}^{\dot{\vartheta}} = 2.1(1 + \frac{30}{s} + \frac{s}{125}) \tag{18}$$

The frequency characteristic curve is shown in Fig. 9

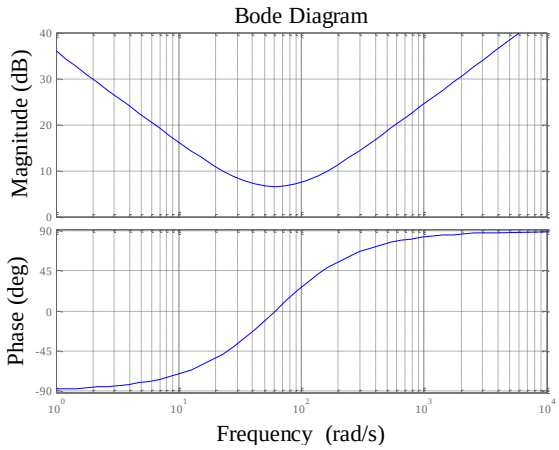


Fig.9 Frequency characteristic of corrective network in pitch damping loop

By substituting the transfer function of the correction network into the damping loop, the frequency characteristic curve of the damping loop can be obtained, as shown in Fig. 10.

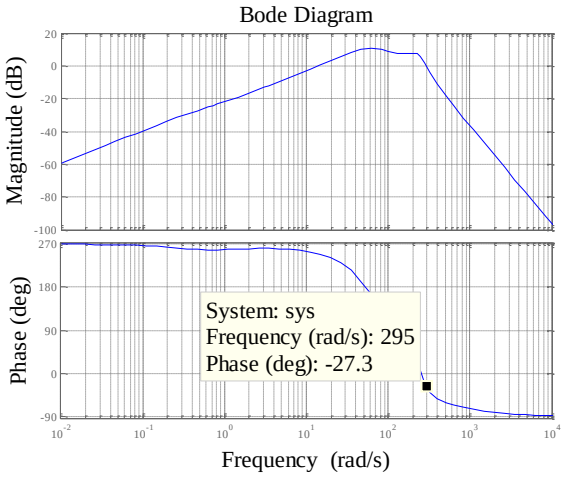


Fig.10 Frequency characteristic of pitch damping loop (corrective network)

It can be seen from Fig. 10 that the phase angle stability margin of damping loop with the addition of correction network is 152.7 deg. On the other hand, the frequency characteristic curve shows that the introduction of correction network does not make the damping loop unstable in frequency domain, which is in accordance with the requirements of the basic design principles.

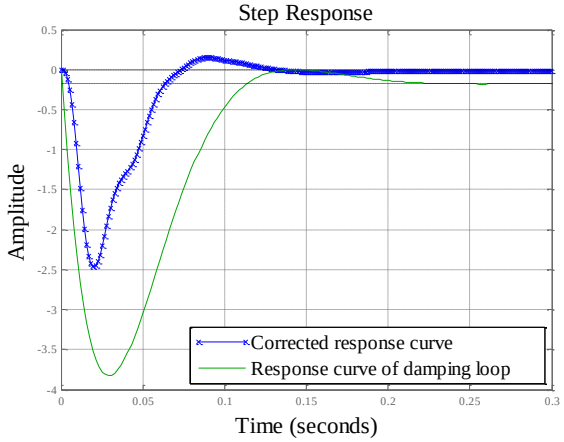


Fig.11 Unit step response curve of pitch channel corrective damping loop

Fig. 11 shows the enlarged unit step response curves of damping loop with and without correction network. Besides, it can be seen that with the addition of the correction network, the steady-state value of unit step response curve of damping circuit further decreases to almost 0, and the peak value of response decreases to -2.5, i.e., a decrease of 37.5%; in the meantime, the time to reach the steady value is shortened from 0.13s to 0.07s.

### *C. Design of overload control loop*

The design of the overload control loop is similar to that of damping loop, which consists of two parts, i.e., the design of gain coefficient and that of corrective network. The structure of the overload control loop is shown in Fig. 12.

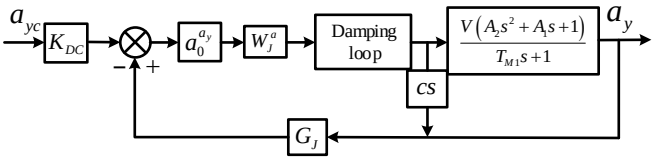


Fig.12 Structure diagram of overload control loop for pitch channel

The unit step response curve of the overload control loop is shown in Fig. 13 in which it can be seen that, under the input condition of unit step response, the overload response is kept at the zero position at the beginning, and then it increases dramatically after 0.27s. In addition, at 0.3s, it can be considered that the overload is infinite, and the missile is out of control.

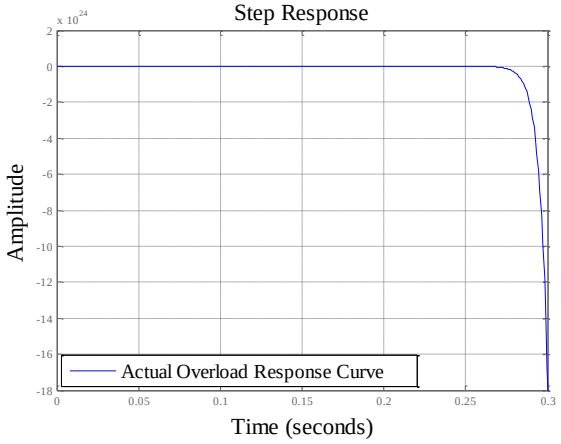


Fig.13 Unit step response curve of overload control loop of pitch channel without gain adjustment

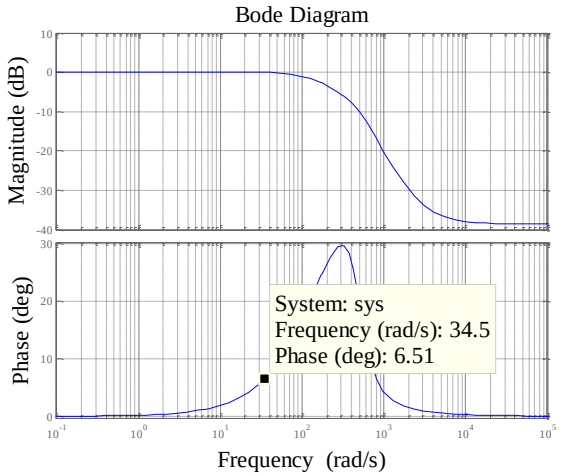


Fig.14 Frequency characteristic curve of overload control loop of pitch channel without gain adjustment

It can be seen from Fig. 14 which shows the frequency characteristic curve of overload control loop without gain regulation, that the phase angle stability margin and amplitude stability margin of overload control loop are 186.51 deg. and 38 dB respectively. Besides, the stability margin meets the requirements of design principle and results in good stability.

Considering that the value of $k_A$ has a great influence on the overshoot and rapidity of the control loop, a design method of the gain coefficient of the control loop using the time domain method is adopted for the optimization of the design of $k_A$ on the basis of the estimated value, and further to make sure that the overshoot of the control loop is low and the response speed is fast.

The basic principle of the design method is described as follows: the control variable $k_A$ which meets the constraints and enjoys the fastest rise time is figured out with $k_A$ as the control variable, the unit step signal as the input, the control loop response as the output and its constraint conditions, and the response rise time as the target value. Fig. 15 shows the control loop response curve with constraints, where $T$ refers to the simulation time, $t_s$ refers to the rise time, $g$ refers to the steady-state value of the response, and 1+$a$, 1+$b$ and 1+$c$ refer to the constraints of the response curve respectively.

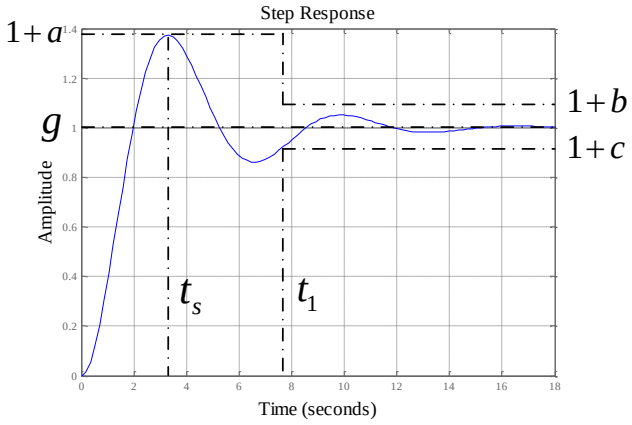


Fig.15 Response and restriction sketch of control loop

It can be seen from Fig. 15 that before $t_1$s, the response of control loop is characterized by only one upper constraint at any time, however, after $t_1$s, the response of control loop is characterized by one upper constraint and one lower constraint at any time. In this way, the optimal design of $k_A$ is converted into a single objective optimization problem under multiple constraints, that is, the optimal $k_A$ is designed to minimize the rise time $t_s$ under the constraint conditions. The optimization process is shown in Fig. 16.

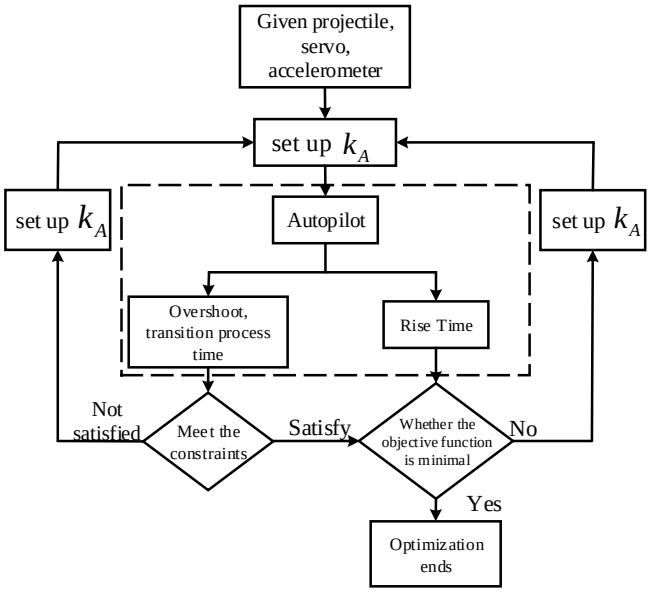


Fig.16 Flowchart of optimization design

During the optimization design process, the overshoot of the overload control loop should be maintained as small as possible to ensure the steady flight of the mortar shell. In that case, the upper constraint value *a* of the control loop response is set to 25%, and *b* is set to 10%; due to the inertia of the steering gear and inertial components, the unit step response of this control loop will jitter at the initial stage. Therefore, $t_1$ is set to 0.16 s and *c* is set to -0.1.

In addition, the adjustment step size of $k_A$ is set to 0.001 to ensure the accuracy of the optimization results and shorten the optimization period.

According to the above optimization design process, and using MATLAB to write the optimization program, we can get that when $k_A = -1/56$, the control loop response amplitude is small, the overshoot is less, and the rise time is short.

With the rise time of 0.06s, the overshoot of 20%, and the overload response amplitude of 0.5, the instability of missile control can be avoided. On the other hand, in the case that the overload is not high, the requirements of missile body control can be met, however, the control efficiency will not be high. At this time, the unit step response curve of overload control circuit is shown in Fig. 17.

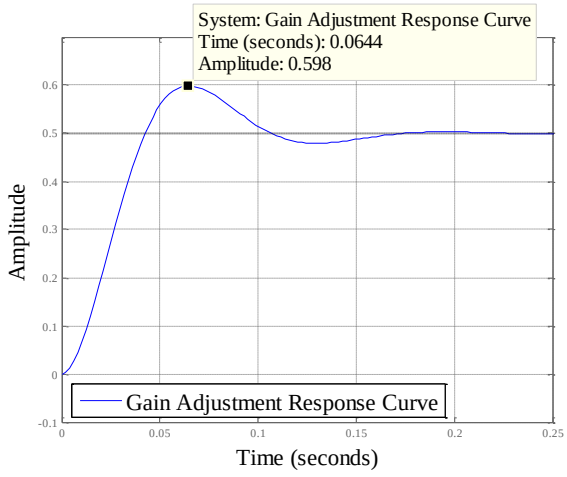


Fig.17 Unit step response curve of overload control loop of pitch channel with gain adjustment

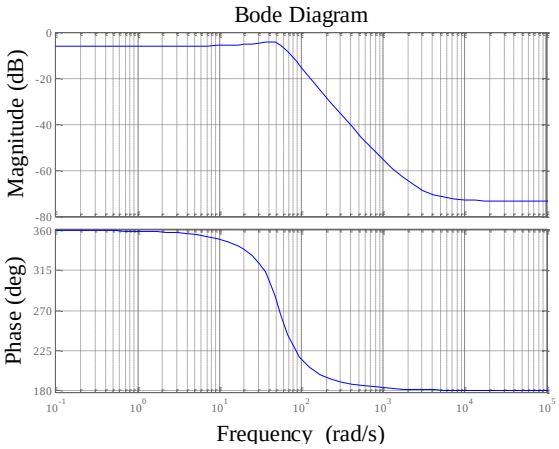


Fig.18 Frequency characteristic curve of overload control loop of pitch channel with gain adjustment

It can be seen from Fig. 18 which shows the frequency characteristic curve of overload control loop after gain adjustment, that after gain correction, the phase stability margin is 540 deg., i.e., an increase of 189.4%. Besides, the amplitude stability margin is 75dB, i.e., an increase of 97.4%. Combined with the unit step response curve, it can be concluded that the response characteristics of overload control loop are greatly improved by gain adjustment.

In the overload control circuit, a correction network in the same form as that of the damping circuit correction network is selected. After repeated calculation, the final overload control loop correction network is expressed as follows:

$$W_J^a = \frac{0.88\left(s^2 + 50s + 1250\right)}{50s} \tag{19}$$

The frequency characteristic curve is shown in Fig. 19.

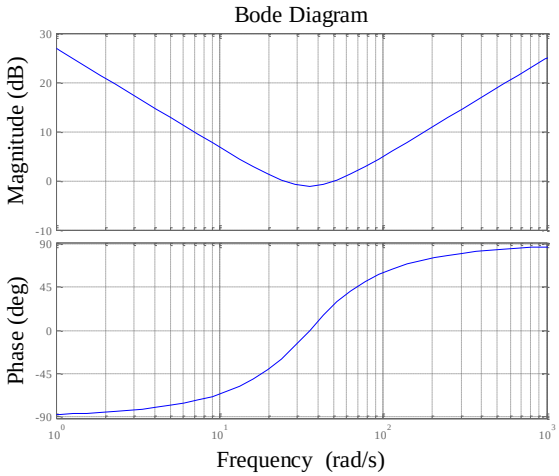


Fig.19 Frequency characteristic of corrective network in pitch overload control

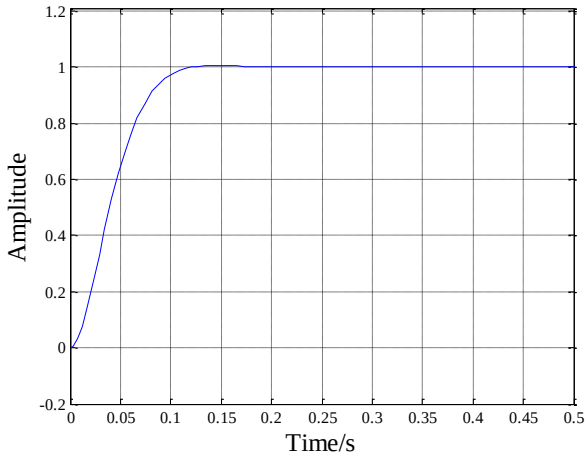


Fig.20 Unit step response curve of overload control loop of pitch channel (with PID corrective network)

The unit response curve of overload control loop corrected by the correction network is shown in Fig. 20. Besides, compared with the response curve without correction network, the overshoot of the curve is reduced to 0%, thus improving the stability of the missile body to overload response, avoiding the excessive response of the missile body, and mitigating the risk of projectile instability. The steady-state value is increased from 0.5 to 1, the efficiency is doubled, and the response time to reach the steady state value is shortened from 0.15s to 0.12s, in this way the response speed of the projectile to overload is improved.

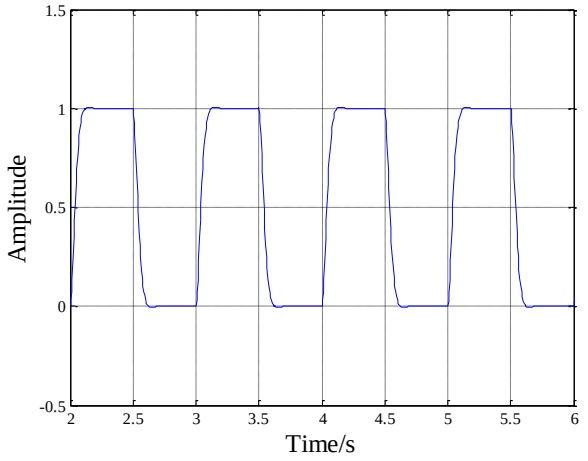


Fig.21 Square wave response curve of overload control loop of pitch channel (with PID corrective network)

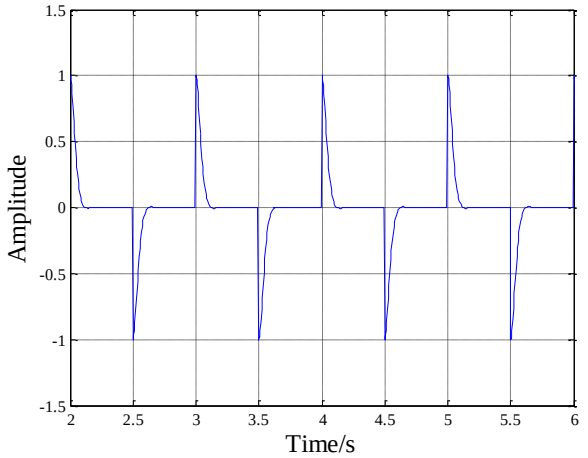


Fig.22 Difference between real square wave and response square wave (with PID corrective network)

The unit step response curve can only reflect the response characteristics of overload control loop to a single overload command. However, in the actual flight process of the missile, the real overload command changes in real time, therefore, square wave is used as overload input to more truly reflect the response of overload control circuit to the changing overload command; besides, the square wave response curve of overload control loop after the addition of correction network is obtained, as shown in Fig. 21. It can be seen from Fig. 21 and Fig. 22 which shows the difference curve between the standard square wave and the response square wave, that the response square wave follows the standard square wave, the two are basically consistent, and the difference is small. Besides, the changing overload command is available for timely response, and the designed overload control pilot is able to meet the actual flight needs of the projectile.

## VI. Conclusion

In this paper, the optimization design of two-loop overload pilot is studied, and the simulation results show that the damping loop is available to effectively suppress the response of angular velocity signal, stabilize the angular velocity of missile body axis in space, and enhance the damping characteristics of angular motion around the mass center. Besides, the overload control is characterized by high response tracking performance to overload command, and fast realization of response without overshoot. From the analysis of frequency domain characteristics, it can be concluded that the amplitude margin and the phase margin of the two-loop pilot is in accordance with the design requirements, and still with enough stability margin reserve in the case of aerodynamic parameters change or external interference; besides, it is characterized by the adaptability under changing environment. The designed two-loop pilot can meet the requirements of guidance ammunition flight stability, which provides theoretical guidance and engineering experience for the pilot design.

## REFERENCES

[1] Ashwini A. Godbole, and S. E. Talole, "Robust Feedback Linearization approach to pitch autopilot design," *In Proceedings of the 2011 7th International Conference on MEMS, NANO and Smart Systems*, 4-6 November, 2012, Switzerland, pp4667-4673.

[2] S. E. Talole, A. A. Godbole, and J. P. Kolhe, "Robust roll autopilot design for tactical missiles," *Journal of Guidance, Control, and Dynamics*, vol. 34, no. 1, pp107-117, 2011.

[3] Negar Elmi Sadr, and Hamid Reza Momeni, "Fuzzy Sliding mode Control for missile autopilot design," *In Proceedings of the 2011 IEEE GCC Conference and Exhibition*, 19-22 February, 2011, pp453-456.

[4] Tine Tomazic, and Drago Matko, "Model based UAV autopilot tuning," *In Proceedings of the 8th WSEAS International Conference on Fluid Mechanics*, 29-31 January, 2011, pp18-22.

[5] Robert F. Hartley, Francois-David X. Hugon, and Richard Anderson, "Development and Flight Testing of a Model Based Autopilot Library for a Low Cost Unmanned Aerial System," *In Proceedings of the AIAA Guidance, Navigation, and Control (GNC) Conference*, 19-22 August, 2013.

[6] Henghao Zhang, "Design of Three-loop Autopilot with Singular Perturbation Margin," *ACTA ARMAMENTARII*, vol. 39, no. 12, pp107-117, 2011.

[7] Yiyang Jiang, "Comparative Study on Three Acceleration Autopilots," *Navigation Positioning & Timing*, vol. 3, no. 1, pp40-46, 2016.

[8] Junfang Fan, and Xin Zhang, "Design Two-loop Autopilot Based on Reinforcement Learning for Miniature Munition," *Tactical Missile Technology*, no. 4, pp48-54, 2019.

[9] Yang Zhang, Fugui Li, and Xinmin Wang, "Robustness Analysis of Three-Loop Acceleration Autopilot," *Aerospace Control*, vol. 35, no. 6, pp26-31, 2017.

[10] Chuncheng Zhou, "Structure Analysis and Design of Three-Loop Autopilot," *Industrial Control Computer*, vol. 30, no. 3, pp60-65, 2017.

[11] Defu Lin, Hui Wang, and Jiang Wang, "Autopilot Design And Guidance Law Analysis For Tactical Missiles," *BEIJING INSTITUTE OF TECHNOLOGY PRESS*, Beijing, China, 2012, pp35-72.

[12] J. Chaoraingern, V. Tipsuwanporn, and A. Numsomran, "Mini-drone Quadrotor Altitude Control Using Characteristic Ratio Assignment PD Tuning Approach," *Lecture Notes in Engineering and Computer Science: Proceedings of The World Congress on Engineering and Computer Science 2019, WCECS 2019*, 22-24 October, 2019, San Francisco, USA, pp337-341.

[13] K. Kankhunthodl, V. Kongratana, and A. Numsomran, et al, "Self-balancing Robot Control Using Fractional-Order PID Controller," *Lecture Notes in Engineering and Computer Science: Proceedings of The International MultiConference of Engineers and Computer Scientists 2019, IMECS 2019*, 13-15 March, 2019, Hong Kong, pp77-82.

[14] Salvador Ramirez, Diego A. Zepeda, and Jaime Cerda et al, "A PID Controller Comparative Study of Tuning Methods for a Three-Phase Induction Motor Speed Control," *Lecture Notes in Engineering and Computer Science: Proceedings of The World Congress on Engineering and Computer Science 2018, WCECS 2018*, 23-25 October, 2018, San Francisco, USA, pp655-659.